Nonspecular effects in the vicinity of a photonic Dirac point

Qiang Yang,[1] Wenhao Xu,[1] Shizhen Chen,[1] Shuangchun Wen,[2] and Hailu Luo[1,*]

[1]*Laboratory for Spin Photonics, School of Physics and Electronics, Hunan University, Changsha 410082, China*

[2]*Key Laboratory for Micro-/Nano-Optoelectronic Devices of Ministry of Education, School of Physics and Electronics, Hunan University, Changsha 410082, China*

(Received 19 October 2020; revised 15 December 2020; accepted 5 February 2021; published 18 February 2021)

Since the construction of various topological photonic metamaterials, the Dirac degeneracy has been realized and provides a crucial opportunity to investigate the nonspecular effects [Goos-Hänchen (GH) and Imbert-Fedorov (IF) shifts] of light at the unique optical interface. In this paper, we furnish a general and precise model to explore how photonic Dirac point affects nonspecular effects in Dirac metamaterial. Based on this model, the giant nonspecular effects are discovered when a Gaussian beam reflects in the vicinity of a photonic Dirac point. We confirm that the giant nonspecular effects are the consequence of degeneracy between Brewster angles and critical angle caused by the Dirac point. Furthermore, the ability to generate a vortex beam at the Dirac point has also been simply verified. We believe that our work is of underlying significance, and may be served as a reference for the measurement of Dirac point, even other degenerate points. Moreover, our precise model can also be used to describe the nonspecular effects in other analogous photonic systems.

DOI: 10.1103/PhysRevA.103.023522

I. INTRODUCTION

Violating the prediction of geometric optics, there exist the longitudinal and transverse shifts in directions parallel and perpendicular to the plane of incidence when a light beam reflects from the dielectric interface, which is deemed to nonspecular effects. In 1947, Goos and Hänchen found longitudinal shift experimentally [1], which was therefore referred to the Goos-Hänchen (GH) shift. Additionally the existence of the GH shift was proved by Artmann in 1948 [2]. The transverse shift was predicted theoretically by Fedorov in 1955 [3] and proved by Imbert in 1972 [4] and so-called Imbert-Fedorov (IF) shift. With the further research, GH and IF angular shifts have also been discovered and extensively studied [5–10]. Although these nonspecular effects have been discovered for decades, the corresponding studies not only touch upon its intrinsic physics [11–16], but also upon various reflected interfaces, such as graphene [17–22], plasmonics [23–25], photonic crystal [26–29], metasurfaces [30,31], weakly absorbing dielectric [32,33], optical waveguide structures [34], and even nonoptical systems [35–38]. In addition, nonspecular effects have potential applications in optical sensors [24,39–41], optical switching [42], beam steering [43], and image edge detection [44]. In topological photonics, the nonspecular effects can be a feasible way of determining the parameters of materials through direct optical measurement [21,45].

In recent years, the emergence of topological materials enriches the classical photonics and plays a significant role to study topological behaviors of electromagnetic waves. Furtherly, the topological insulators [46–48], Weyl degeneracies [49–51], and Dirac degeneracies [52–54] have been realized theoretically and experimentally in the metamaterial and photonic crystal systems. Hence, the research of nonspecular effects based on topological materials, such as topological insulators [55], Weyl semimetals in photonic system [56], and electronic system [37,38], has attracted much attention of scholars. In photonics, fourfold degeneracy of the Dirac point can be realized through spatial degrees of freedom [57,58] or the intrinsic degrees of freedom in electromagnetism under electromagnetic duality [54]. Additionally, the basic topology is connected between a Dirac point and vortex or vector beams [54], and a strong photonic spin Hall effect near the Dirac point occurs when a Gaussian beam impinges on the interface of photonic Dirac metamaterial [59]. Owing to the particularity of Dirac point, we are interested in the question of how it affects nonspecular effects in light reflection.

Herein, a general and precise model is established to describe the nonspecular effects at the interface of photonic Dirac metamaterial. In our model, the cross-polarization components of reflection coefficients appear when the reflection behavior of arbitrary wave vector is considered. In Dirac metamaterial, the giant nonspecular effects can be found when a Gaussian beam reflects in the vicinity of a photonic Dirac point. We underline that it is the Dirac point that ties the Brewster angles and critical angle together to achieve degeneracy, which results in both giant GH and IF shifts near the Dirac point. In addition, the ability to generate a vortex beam at the Dirac point has also been simply verified. Hence, the degeneracy of Dirac point paves a new way to generate vector and vortex beams [54]. Finally, we show that as the beam waist of incident beam increases to a sufficiently large value, the beam shifts reach the asymptotic regime. In this case, the beam width is so large that the related effects are difficult to measure [67,68].

*hailuluo@hnu.edu.cn

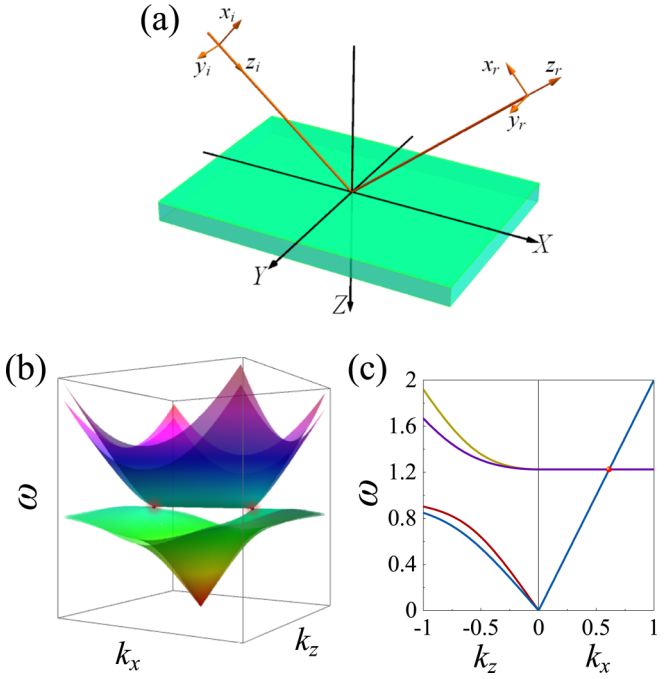

FIG. 1. (a) Schematic illustrating the Cartesian coordinate system in Dirac metamaterial. (b) Band structure on the k_x-k_z plane with $\varepsilon_y = \mu_y = 0.5$. (c) The dispersion relation along the k_x and k_z directions, respectively. In both (b) and (c), the Dirac points are marked with red spheres.

II. BAND STRUCTURE AND FRESNEL EQUATIONS IN DIRAC METAMATERIAL

We first set up the Cartesian coordinate system (x, y, z) in the photonic Dirac metamaterial, and use coordinate frame (x_i, y_i, z_i) and coordinate frame (x_r, y_r, z_r) to denote the central wave vectors of incidence and reflection, respectively [see Fig. 1(a)]. Then we consider a uniaxial metamaterial with homogeneous effective electromagnetic properties. The effective parameters of the medium have the anisotropic form $\bar{\varepsilon} = \mathrm{diag}[\varepsilon_x, \varepsilon_y, \varepsilon_z]$ and $\bar{\mu} = \mathrm{diag}[\mu_x, \mu_y, \mu_z]$. In our model, there are $\varepsilon_y = \varepsilon_z = \text{const}$, $\mu_y = \mu_z = \text{const}$, and

$$\varepsilon_x = 1 + f_1\omega_0^2/\left(\omega_0^2 - \omega^2\right), \quad \mu_x = 1 + f_2\omega^2/\left(\omega_0^2 - \omega^2\right), \tag{1}$$

where ω_0 is the resonance frequency and the coefficients f_1 and f_2 are adjustable constants determined by the structure parameters. The resonance along x direction of permittivity and permeability means that there exist two bulk plasmon modes, a longitudinal electric mode, and a longitudinal magnetic mode. The degeneracy between the two longitudinal modes can be reached by setting $f_2 = 1 - 1/(1 + f_1)$. Moreover, the feasibility of a realistic metamaterial structure was theoretically proposed [54] and experimentally fabricated [60].

To obtain the band structure of photonic Dirac metamaterial, we commence from Maxwell's equations:

$$\nabla \times \mathbf{E} = i\omega\mathbf{B}, \tag{2}$$

$$\nabla \times \mathbf{H} = -i\omega\mathbf{D}. \tag{3}$$

Multiply $\nabla \times \bar{\mu}^{-1}$ on both sides of Eq. (2) and $\nabla \times \bar{\varepsilon}^{-1}$ on both sides of Eq. (3), and utilize the constitutive relations: $\mathbf{D} = \bar{\varepsilon}\mathbf{E}$, $\mathbf{B} = \bar{\mu}\mathbf{H}$, we have wave equations of electric and magnetic fields:

$$\nabla \times \bar{\mu}^{-1}(\nabla \times \mathbf{E}) = \bar{\varepsilon}\omega^2\mathbf{E}, \tag{4}$$

$$\nabla \times \bar{\varepsilon}^{-1}(\nabla \times \mathbf{H}) = \bar{\mu}\omega^2\mathbf{H}. \tag{5}$$

Assuming that electromagnetic fields $\mathbf{E}$ and $\mathbf{H}$ possess the form $e^{i\mathbf{k}\cdot\mathbf{r}}$, then the wave equations can be rewritten as $\bar{M}\mathbf{E} = 0$ and $\bar{N}\mathbf{H} = 0$, where

$$\bar{M} = (\mathbf{k} \times \bar{I})\bar{\mu}^{-1}(\mathbf{k} \times \bar{I}) + \omega^2\bar{\varepsilon}, \tag{6}$$

$$\bar{N} = (\mathbf{k} \times \bar{I})\bar{\varepsilon}^{-1}(\mathbf{k} \times \bar{I}) + \omega^2\bar{\mu}, \tag{7}$$

and $\bar{I}$ is the identity tensor.

The zero determinant of 3×3 matrix $\bar{M}$ and $\bar{N}$ can give rise to the characteristic equation. After substituting permittivity and permeability in Eq. (1) into the characteristic equation, the band structure of photonic Dirac metamaterial can be deduced, as shown in Figs. 1(b) and 1(c). Figure 1(b) shows the band structure of bulk states in the k_x-k_z plane, where two bands are nearly overlapping with each other. In the direction of k_x, there are two fourfold degeneracy points named Dirac points symmetrically displaced, as marked with the red spheres. Figure 1(c) presents the dispersion relation of the material along the k_x and k_z directions. We can get the Dirac points (k_D, ω_D) with $k_D = \pm k_0\sqrt{\varepsilon_y\mu_y}$ and $\omega_D = \sqrt{1 + f_1}\omega_0$, where $k_0 = \omega/c$ is the the wave number in vacuum, and c is the speed of light.

We consider a Gaussian beam of frequency ω impinges on the interface between vacuum and Dirac metamaterial at an angle θ_i to obtain the Fresnel equations. The Gaussian beam is a superposition of different plane waves, and the direction of the optical axis for arbitrary wave vector is not identical. Then we introduce a unit vector $\hat{I}$:

$$\hat{I} = \alpha\hat{\mathbf{x}} + \beta\hat{\mathbf{y}} + \gamma\hat{\mathbf{z}}, \tag{8}$$

and let α, β, γ be direction cosines of the optical axis relative to the Cartesian laboratory frame. For an arbitrary direction of optical axis, the tensors of permittivity and permeability can be amended as [61]

$$\bar{\varepsilon} = \begin{bmatrix} \varepsilon_y + \alpha^2\Delta\varepsilon & \alpha\beta\Delta\varepsilon & \alpha\gamma\Delta\varepsilon \\ \alpha\beta\Delta\varepsilon & \varepsilon_y + \beta^2\Delta\varepsilon & \beta\gamma\Delta\varepsilon \\ \alpha\gamma\Delta\varepsilon & \beta\gamma\Delta\varepsilon & \varepsilon_y + \gamma^2\Delta\varepsilon \end{bmatrix}, \tag{9}$$

$$\bar{\mu} = \begin{bmatrix} \mu_y + \alpha^2\Delta\mu & \alpha\beta\Delta\mu & \alpha\gamma\Delta\mu \\ \alpha\beta\Delta\mu & \varepsilon_y + \beta^2\Delta\mu & \beta\gamma\Delta\mu \\ \alpha\gamma\Delta\mu & \beta\gamma\Delta\mu & \varepsilon_y + \gamma^2\Delta\mu \end{bmatrix}, \tag{10}$$

with $\alpha^2 + \beta^2 + \gamma^2 = 1$ due to the unit vector $\hat{I}$, and $\Delta\varepsilon = \varepsilon_x - \varepsilon_y$, $\Delta\mu = \mu_x - \mu_y$.

Let the xz plane be the incident plane, the optical axis is almost along the x direction in the xy plane, that is $\alpha \to 1$, $\gamma = 0$. The direction cosine β can be indicated by k_{iy}, which respects the y component of arbitrary vector relative to the beam center, hence there is $\beta \sim k_{iy}/k_i \sin\theta_i$. In Dirac metamaterial, for a given incident wave vector $\mathbf{k} = (k_x, 0, k_z)$, there are two

normal wave vector components $k_z^{\pm}$. The corresponding transmitted electromagnetic fields are the eigenstates determined by the null space of the Hamiltonian formalism $\bar{M}$ and $\bar{N}$ (see Appendix A).

By utilizing the boundary conditions [62] and considering the paraxial approximation (see Appendix A), the Fresnel reflection coefficients can be deduced as

$$r_{pp} = \frac{-q_e + \varepsilon_x \cos\theta_i}{q_e + \varepsilon_x \cos\theta_i}, \tag{11}$$

$$r_{ss} = \frac{-q_o + \mu_x \cos\theta_i}{q_o + \mu_x \cos\theta_i}, \tag{12}$$

$$r_{ps} = \frac{2\frac{k_{iy}}{k_i}\sqrt{\varepsilon_x\mu_x}(\sqrt{\varepsilon_x\mu_x} - \sqrt{\varepsilon_y\mu_y})\cot\theta_i}{(q_e + \varepsilon_x\cos\theta_i)(q_o + \mu_x\cos\theta_i)}, \tag{13}$$

$$r_{sp} = \frac{2\frac{k_{iy}}{k_i}\sqrt{\varepsilon_x\mu_x}(\sqrt{\varepsilon_y\mu_y} - \sqrt{\varepsilon_x\mu_x})\cot\theta_i}{(q_e + \varepsilon_x\cos\theta_i)(q_o + \mu_x\cos\theta_i)}, \tag{14}$$

where r_{pp}, r_{ss}, and $r_{ps}(r_{sp})$ represent the Fresnel reflection coefficients for parallel, perpendicular, and crossing polarization, respectively. Considering the robustness of our model, if we set $\varepsilon_x = \varepsilon_y = \text{const}$ and $\mu_x = \mu_y = 1$, the reflection coefficients Eqs. (11)−(14) can reproduce to the classical case of isotropic [63]. Accordingly, this general and precise model can be used in other similar systems based on a real Gaussian beam transmission. It should be noted, moreover, that if the reflection of arbitrary wave vector is not taken into consideration, there will be no reflection coefficients r_{ps} and r_{sp} for crossing polarizations.

III. GIANT NONSPECULAR EFFECTS

In this section, we will establish a general and precise model to describe nonspecular effects of the light beam at the interface of photonic Dirac metamaterial. The angular spectrums of the reflected field and the incident field are linked by the reflection matrix:

$$\begin{bmatrix} \tilde{E}_r^p \\ \tilde{E}_r^s \end{bmatrix} = \begin{bmatrix} r_{pp} & r_{ps} \\ r_{sp} & r_{ss} \end{bmatrix} \cdot \begin{bmatrix} \tilde{E}_i^p \\ \tilde{E}_i^s \end{bmatrix}. \tag{15}$$

We consider a monochromatic Gaussian beam with finite beam width impinging from air to a planar interface of Dirac metamaterial. The incident angular spectrum of a Gaussian beam can be written as

$$\tilde{E}_i(k_{ix}, k_{iy}) = (f_p\hat{\mathbf{x}}_i + f_s\hat{\mathbf{y}}_i)\exp\left[-\frac{{w_0}^2\left({k_{ix}}^2 + {k_{iy}}^2\right)}{4}\right], \tag{16}$$

where $f_p = a_p \in \mathbb{R}$ and $f_s = a_s\exp(i\eta)$, which determine the polarization of the beam and w_0 is the beam waist. The complex amplitude for the reflected beam in position space can be expressed by utilizing the Fourier transformation:

$$\mathbf{E}_r(x_r, y_r, z_r) = \iint dk_{rx}dk_{ry}\tilde{E}_r(k_{rx}, k_{ry}) \times \exp[i(k_{rx}x_r + k_{ry}y_r + k_{rz}z_r)], \tag{17}$$

where $k_{rz} = \sqrt{k_r^2 - (k_{rx}^2 + k_{ry}^2)}$ which can be expanded to the first order in the paraxial optics: $k_{rz} \sim -(k_{rx}^2 + k_{ry}^2)/2k_0$. $\tilde{E}_r(k_{rx}, k_{ry})$ is the reflected angular spectrum that can be obtained by combining the Eqs. (15), (16), and the boundary conditions: $k_{rx} = -k_{ix}$ and $k_{ry} = k_{iy}$.

The GH and IF shifts of beam occur in the directions parallel and perpendicular to the plane of incidence, respectively. At any given plane $z_r = \text{const}$, the GH and IF shifts can be obtained by giving the field centroid of longitudinal and transverse displacements:

$$D_{\text{GH}} = \frac{\iint x_r I(x_r, y_r, z_r)dx_r dy_r}{\iint I(x_r, y_r, z_r)dx_r dy_r}, \tag{18}$$

$$D_{\text{IF}} = \frac{\iint y_r I(x_r, y_r, z_r)dx_r dy_r}{\iint I(x_r, y_r, z_r)dx_r dy_r}. \tag{19}$$

The intensity distribution of beam is closely related to the Poynting vector $I(x_r, y_r, z_r) \propto \mathbf{S}\cdot\hat{\mathbf{z}}_r$. Then the Poynting vector associated with the electromagnetic field can be shown as $\mathbf{S} \propto \text{Re}(\mathbf{E}_r \times \mathbf{H}_r^*)$, where the magnetic field is given by $\mathbf{H}_r = -ik_r^{-1}\nabla \times \mathbf{E}_r$.

For GH shift, we consider an incident beam with horizontal polarization (HP), i.e., $a_p = 1$, $a_s = 0$, and $\eta = 0$. Then the expression of GH shift can be derived (see Appendix B for detailed derivations) as

$$\Delta_{\text{GH}}^H = \frac{2z_R R_{pp}^2 \varphi_{pp}}{R_{sp}'^2 + 2k_0 z_R R_{pp}^2 + \chi_{pp}}, \tag{20}$$

$$\Theta_{\text{GH}}^H = -\frac{2R_{pp}^2 \rho_{pp}}{R_{sp}'^2 + 2k_0 z_R R_{pp}^2 + \chi_{pp}}, \tag{21}$$

where $r_A = R_A\exp(i\phi_A)$, $\rho_A = \text{Re}(\partial \ln r_A/\partial\theta_i)$, $\varphi_A = \text{Im}(\partial \ln r_A/\partial\theta_i)$, $\chi_A = R_A^2(\varphi_A^2 + \rho_A^2)$, $z_R = k_0 w_0^2/2$ is the Rayleigh length and the notations Δ and Θ denote the spatial shift and angular shift, respectively. The GH shift of vertical polarization (i.e., $a_p = 0$, $a_s = 1$, and $\eta = 0$) can be obtained by replacing r_{pp} and r_{sp} with r_{ss} and r_{ps}, respectively.

Similarly for IF shift, we consider an incident beam with left-handed circular polarization (LCP), i.e. $a_p = 1/\sqrt{2}$, $a_s = 1/\sqrt{2}$, and $\eta = \pi/2$, then the spatial and angular shifts can be obtained (see Appendix B for detailed calculations) as

$$\Delta_{\text{IF}}^L = \frac{2z_R[\xi_1 - \xi_2 + \zeta\cot\theta_i]}{R_{ps}'^2 + R_{sp}'^2 + 2k_0 z_R\left(R_{pp}^2 + R_{ss}^2\right)}, \tag{22}$$

$$\Theta_{\text{IF}}^L \approx 0, \tag{23}$$

where $\xi_1 = R_{sp}'R_{ss}\cos(\phi_{sp} - \phi_{ss})$, $\xi_2 = R_{ps}'R_{pp}\cos(\phi_{ps} - \phi_{pp})$, $\zeta = R_{pp}^2 + R_{ss}^2 + 2R_{pp}R_{ss}\cos(\phi_{pp} - \phi_{ss})$, $r_A = R_A\exp(i\phi_A)$. Likewise, we can get the IF shift for an incident beam with right-handed circular polarization (RCP) (i.e., $a_p = 1/\sqrt{2}$, $a_s = 1/\sqrt{2}$, and $\eta = -\pi/2$) as $\Delta_{\text{IF}}^R = -\Delta_{\text{IF}}^L$ and $\Theta_{\text{IF}}^R = -\Theta_{\text{IF}}^L \approx 0$. Hence, for both LCP and RCP, there is nearly no IF angular shift occurs at the interface of the Dirac metamaterial.

In the following discussion, we will choose (θ_D, ω_D) to denote the Dirac point owing to the relation $k_D = k_0\sqrt{\varepsilon_y\mu_y}$ and the incident condition $k_i = k_0 = k_D/\sin\theta_D$. As illustrated in Fig. 2, 3D figures of the GH and IF shifts are plotted as the functions of the distance $\delta\theta_i$ away from Dirac angle θ_D and the distance $\delta\omega$ away from the Dirac frequency ω_D. The giant GH spatial and angular shifts with HP incidence [see Figs. 2(a) and 2(b)] and giant IF spatial shift with LCP

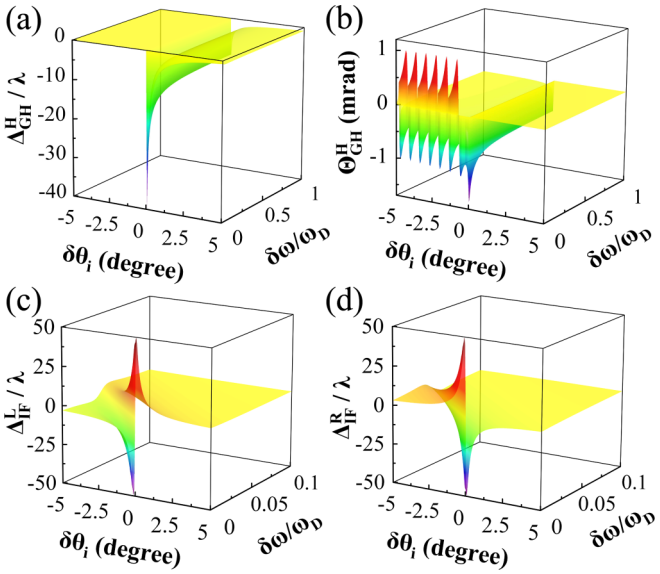

FIG. 2. The GH and IF shifts are plotted as the functions of the distance $\delta\theta_i$ away from Dirac angle θ_D and the distance $\delta\omega$ away from the Dirac frequency ω_D on the surface of Dirac metamaterial. (a) GH spatial shift with HP incidence. (b) GH angular shift with HP incidence. (c) IF spatial shift with LCP incidence. (d) IF spatial shift with RCP incidence. We set the incident beam with horizontal polarization for GH shift and circular polarization for IF shift, waist radius $w_0 = 100 \times \lambda$, and $\lambda = 2\pi c/\omega$. Parameters for the Dirac metamaterial are chosen as $\varepsilon_y = \mu_y = 0.5$ and structural coefficient $f_1 = 0.5$.

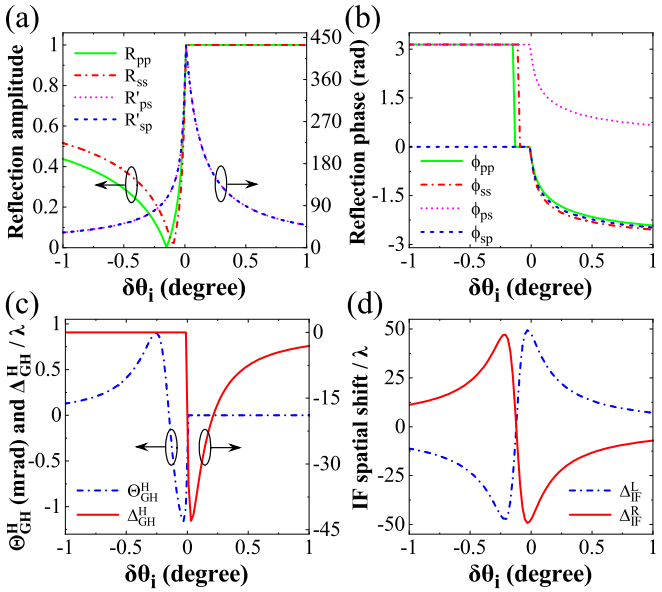

FIG. 3. The reflection coefficients, GH and IF shifts near the Dirac point. (a) Reflection amplitude. (b) Reflection phase. (c) GH spatial and angular shifts with HP incidence. (d) IF spatial shifts with LCP and RCP incidence. The frequency of the incident beam is $\delta\omega = 10^{-3}\omega_D$. Other parameters are the same as those in Fig. 2.

and RCP incidence [see Figs. 2(c) and 2(d)] which are very sensitive to the change of incident angles can be obtained when a Gaussian beam reflects near the Dirac point. For GH spatial and angular shifts, only one of them appears under the same incident condition. In Fig. 2(b), the jagged GH angular shift when $\delta\theta_i < 0^\circ$ is caused by Brewster angle at different frequencies. We believe that the result of this giant nonspecular effects is of underlying significance, and may be served as a reference for the optical measurement of Dirac point, even other degenerate points.

In order to reveal the origin of giant nonspecular effects in the vicinity of a photonic Dirac point, we discuss the reflection amplitude and phase plotted in Figs. 3(a) and 3(b) as the functions of the distance $\delta\theta_i$ away from Dirac angle θ_D, and we choose the frequency as $\delta\omega = 10^{-3}\omega_D$. It can be seen that the Brewster angles appear near the Dirac angle and reflection amplitude R_{ps}, R_{sp} have a peak at the Dirac angle and reflection phase ϕ_{pp}, ϕ_{ss} have a saltation at the Brewster angles. It is worth mentioning that both GH shift and IF shift are zero at the Brewster angle because of the zero reflection coefficients. Furthermore, the Dirac angle coincides with the critical angle. Consequently, the giant GH spatial shift occurs near the Dirac angle, giant GH angular shift and IF spatial shift occur near the Brewster angles due to the distortion of the reflection fields near these angles, as shown in Figs. 3(c) and 3(d). Such enhancement near the Brewster angle has also been demonstrated in other systems [17,22,64–66].

As mentioned above that the Brewster angles appear near the Dirac angle, hence we are interested in the connection between Dirac point, Brewster angles, and critical angle. According to the Eqs. (17) and (18), we can obtain the Brewster angles θ_B and θ_B' for parallel and perpendicular polarization, respectively:

$$\theta_B = \arccos\sqrt{\frac{1-\varepsilon_y\mu_y}{1-\varepsilon_x\varepsilon_y}}, \tag{24}$$

$$\theta_B' = \arccos\sqrt{\frac{1-\varepsilon_y\mu_y}{1-\mu_x\mu_y}}, \tag{25}$$

where ε_y and μ_y are the constants, $\varepsilon_x = 1 + f_1\omega_0^2/(\omega_0^2 - \omega^2)$ and $\mu_x = 1 + f_2\omega^2/(\omega_0^2 - \omega^2)$ are longitudinal electric mode and longitudinal magnetic mode, respectively. Based on the degeneracy condition $f_2 = 1 - 1/(1 + f_1)$ of two longitudinal modes, at the Dirac point, there are $\varepsilon_x = 0$ and $\mu_x = 0$. Therefore, the Brewster angles $\theta_B = \theta_B' = \arccos\sqrt{1-\varepsilon_y\mu_y}$. In addition, the critical angle and Dirac angle are degenerate due to the model itself:

$$\theta_C = \theta_D = \arcsin\sqrt{\varepsilon_y\mu_y}. \tag{26}$$

Notice that $\arccos\sqrt{1-\varepsilon_y\mu_y} = \arcsin\sqrt{\varepsilon_y\mu_y}$ by mathematical derivation. Hence, at the Dirac point, the Brewster angles and critical angle are degenerate (that is $\theta_B = \theta_B' = \theta_C = \theta_D$).

As shown in the Fig. 4(a), when the incident frequency reduces to the Dirac frequency (that is $\delta\omega/\omega_D = 0$), the Brewster angles approach the Dirac point (as marked with a green spot) and therefore meet the critical angle. We confirm, thus, that it is the Dirac point that connects the Brewster angles and critical angle together to achieve degeneracy, thereby resulting in both giant GH and IF shifts near the Dirac point. It can also be well verified from Figs. 4(b)–4(e) that giant GH spatial shift occurs near the critical angle, giant GH angular shift

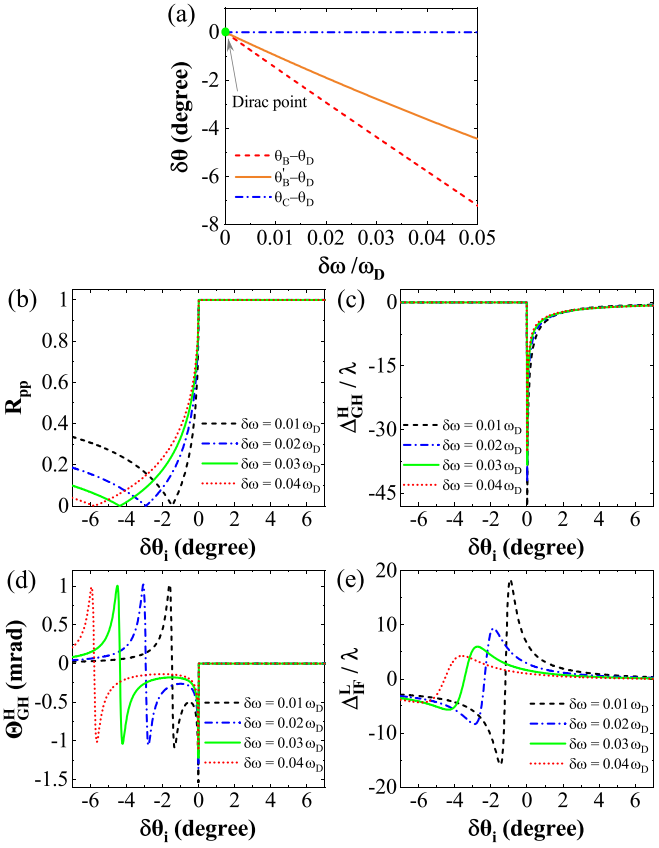

FIG. 4. The influence mechanism of Dirac point on nonspecular effects. (a) The connection between Dirac point, Brewster angles, and critical angle. The Dirac point (θ_D, ω_D) is marked with a green spot. (b) Brewster angle θ_B with the different frequencies. (c) GH spatial shift. (d) GH angular shift. (e) IF spatial shift. We set the frequency change as $\delta\omega/\omega_D = 0.01, 0.02, 0.03, 0.04$. Other parameters are the same as those in Fig. 2.

occurs near the Brewster angle and critical angle, giant IF spatial shift occurs near the Brewster angle. Importantly, it can be clearly seen that as the Brewster angle approaches the Dirac point, the giant shifts tend to the Dirac point.

The reflection field intensity distributions of GH shift with HP incidence and IF shift with LCP incidence are shown in Figs. 5(a) and 5(b), respectively. The incident angle $\delta\theta_i$ is 0.03° for GH shift and -0.03° for IF shift, and we set the incident frequency $\delta\omega = 10^{-3}\omega_D$. Obviously, the GH and IF shifts emerge in the directions parallel $(\hat{\mathbf{x}}_r)$ and perpendicular $(\hat{\mathbf{y}}_r)$ to the plane of incidence, respectively. The distance between the centroid of the light spot and the vertical (horizontal) dashed white line corresponds to the GH (IF) spatial shift. The reflected angular spectrum is highly asymmetric and no longer possess a intact Gaussian distribution. This deformed angular spectrum caused by the Dirac point is completely coherent with the results of shift curves in Figs. 3(c) and 3(d). It is the Dirac point that results in the degeneracy of Brewster angle and critical angle, thereby leading to this giant nonspecular effects. Figures 5(c) and 5(d) give the reflected phase and intensity distribution of reflected field in the vicinity of a Dirac point $(\delta\theta_i = -0.0012^\circ,\ \delta\omega = 10^{-5}\omega_D)$ with LCP incidence, respectively. Circular polarizations are the

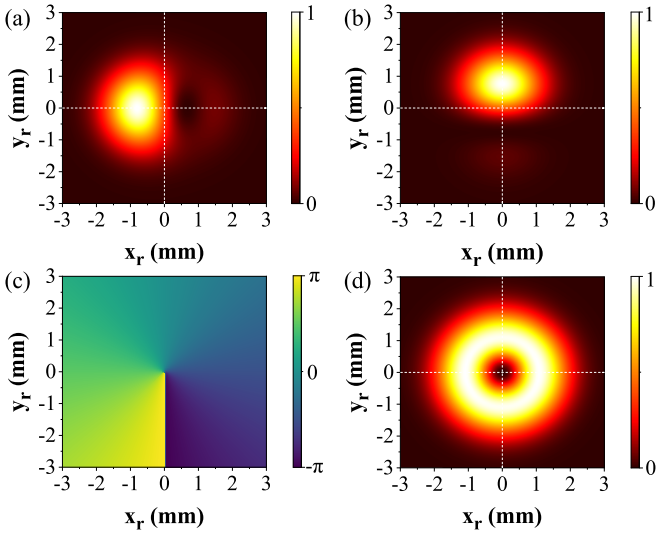

FIG. 5. The reflected field intensity distributions and phase. (a) and (b) show the field intensity distribution with HP incidence for GH shift and LCP incidence for IF shift, respectively. (c) and (d) give the reflected helical phase and intensity distribution of reflected vortex field near the Dirac point$(\delta\theta_i = -0.0012^\circ, \delta\omega = 10^{-5}\omega_D)$ with LCP incidence.

eigenstates of the system because of the electromagnetic duality. In the position space, a counterclockwise helical phase 2π appears [see Fig. 5(c)] with LCP incidence leading to the generation of a vortex beam [see Fig. 5(d)] in reflection in the vicinity of a Dirac point. Hence, the degeneracy of Dirac point provides a novel method to generate vector and vortex beams [54].

Now, to explore the role of the cross-polarization components of reflection matrix in beam shifts, we set $R'_{ps} = 0$ and $R'_{sp} = 0$ in reflection matrix, and this can also be achieved in experiment by utilizing a polarizer to eliminate the cross-polarization components. Then we obtain the modified GH and IF shifts as

$$\Delta_{\mathrm{GH}}^{H'} = \frac{2z_R R_{pp}^2 \varphi_{pp}}{2k_0 z_R R_{pp}^2 + \chi_{pp}}, \tag{27}$$

$$\Theta_{\mathrm{GH}}^{H'} = -\frac{2R_{pp}^2 \rho_{pp}}{2k_0 z_R R_{pp}^2 + \chi_{pp}}, \tag{28}$$

$$\Delta_{\mathrm{IF}}^{L'} = -\frac{\left[R_{pp}^2 + R_{ss}^2 + 2R_{pp}R_{ss}\cos(\phi_{pp} - \phi_{ss})\right]\cot\theta_i}{k_0\left(R_{pp}^2 + R_{ss}^2\right)}, \tag{29}$$

$$\Theta_{\mathrm{IF}}^{L'} = 0. \tag{30}$$

Note that if the cross-polarization of reflection matrix is not considered, both GH and IF shifts [see Eqs. (27)–(30)] can be consistent with the result in Ref. [56].

In Fig. 6, we give the GH and IF spatial shifts for cross-polarization components considered (solid blue line) and not considered (dashed red line). The intensity distributions of reflected field for two different expressions are also inserted in the figure. The position pointed by the arrow corresponds to the incident condition and also the result of it. In Fig. 6(b), it can be seen that without the contribution of the

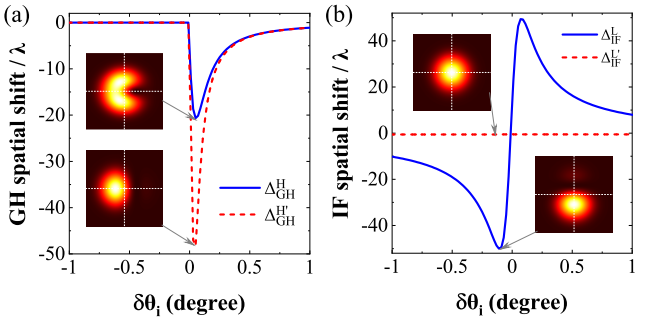

FIG. 6. The GH and IF spatial shifts are obtained from two different expressions for cross-polarization components considered (solid blue line) and not considered (dashed red line). (a) GH spatial shift. (b) IF spatial shift. Insets show the intensity distributions of the reflected field for two different expressions. The position pointed by the arrow corresponds to the incident condition and also the result of it. We set the change $\delta\omega/\omega_D = 10^{-4}$. Other parameters are the same as those in Fig. 2.

cross-polarization components, the IF spatial shift is almost zero (see dashed red line). Accordingly, there exist huge disparity for two different cases and the cross-polarization components of the reflection coefficients which are small quantities have a great influence on the nonspecular effects. For a real Gaussian beam, the directions of optical axis for different wave vectors are not identical, so the reflection behavior of arbitrary wave vector that previous works did not involve in the question of nonspecular effects should be taken into account. Hence, our Fresnel equation model in Eqs. (11)–(14) is more precise to study the nonspecular effects at the interface of bulk crystals.

In the above investigation, we focus on the GH and IF shifts at the interface between the Dirac metamaterial and air under a certain incident beam width. However, this nonspecular effects depend on the incident beam waist when the beam width is in a relatively narrow range. The GH and IF shifts reach the asymptotic regime and only incident angle dependent when the beam waist is large enough, as shown in Fig. 7. Figures 7(a)–7(c) are GH spatial shift, GH angular shift, and IF spatial shift as a function of the incident beam waist for two selected incident angles, respectively. In the range of narrow beam waist, the shifts corresponding to the two selected angles are not significantly different because of a 0.03° incident angle change only. It is worth noting that the GH angular shift tends to zero in the scale of large beam waist [see Fig. 7(b)]. Because in this case, the divergence of a beam is extremely prosperous.

From Eqs. (20)−(22), the large beam waist means $2k_0 z_R R_{pp}^2 \gg (R_{sp}'^2 + \chi_{pp})$ and $2k_0 z_R (R_{pp}^2 + R_{ss}^2) \gg (R_{sp}'^2 + R_{ps}'^2)$, then a straightforward calculation yields: $\Delta_{\mathrm{GH}}^{H''} = \varphi_{pp}/k_0$ which coincides well with the Artmann formula [2], $\Theta_{\mathrm{GH}}^{H''} = -\rho_{pp}/k_0 z_R$ which agrees with the theoretical result of Aiello [11], and $\Delta_{\mathrm{IF}}^{L''} = \Delta_{\mathrm{IF}}^{L'}$. It is clear that these asymptotic formulas can be fully trusted only when the beam waist is extremely wide rather than narrow. The asymptotic results are interesting and valid. However, as enormous beams are required to reach the asymptotic regime, the related effects may be intractable to observe [67,68].

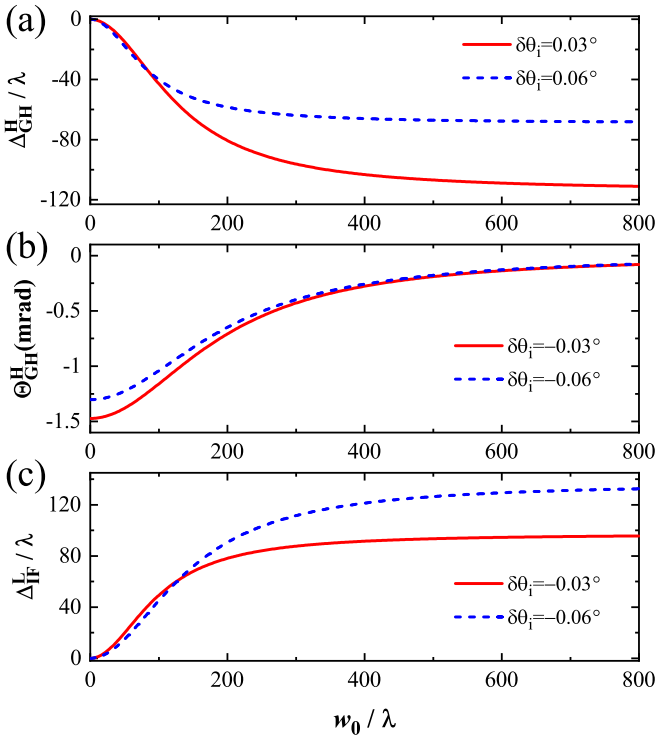

FIG. 7. The GH spatial shift (a), GH angular shift (b), and IF spatial shift (c) change as a function of the incident beam waist for two different incident angles. We choose the frequency of beam as $\delta\omega/\omega_D = 10^{-3}$.

IV. CONCLUSIONS

In conclusion, we have established a general and precise model to explore how photonic Dirac point affects nonspecular effects of the light beam in photonic Dirac metamaterial. By considering the reflection behavior of arbitrary wave vector, the cross-polarization components of the reflection coefficients appear and have a great influence on nonspecular effects. It is demonstrated that the giant nonspecular effects which are very sensitive to the incident angles occur when a Gaussian beam reflects in the vicinity of a photonic Dirac point. We underline that the giant nonspecular effects near the Dirac point are the consequence of degeneracy between Brewster angles and critical angle caused by the Dirac point. Furthermore, it is simply verified that the degeneracy of Dirac point provides a new path to generate vector and vortex beams. We believe that the result of giant nonspecular effects near the Dirac point is of underlying significance, and may be served as a reference for the optical measurement of Dirac point, even other degenerate points. Moreover, the nonspecular effects in other analogous photonic systems can also be investigated by our precise model.

ACKNOWLEDGMENTS

We are sincerely grateful to the anonymous referee, whose comments have led to a significant improvement of our paper. This research was supported by the National Natural Science Foundation of China (Grants No. 11904097 and No. 61835004).

APPENDIX A: FRESNEL REFLECTION COEFFICIENTS

In this Appendix, we give the specific derivation of the Fresnel reflection coefficients, which retain robustness and accuracy and can be used in other similar bulk materials based on a real Gaussian beam transmission. The Gaussian beam is a superposition of different plane waves, and the direction of the optical axis for each wave vector is not identical. Therefore the reflection behavior of arbitrary wave vector is taken into account [see Eqs. (8)–(10)].

Substituting Eqs. (9) and (10) into Eq. (6) and solving the characteristic equation $|\bar{M}| = 0$, there are two normal wave vector components:

$$k_z^+ = \sqrt{\frac{-k_x^2(\Delta\varepsilon + \varepsilon_y) + k_0^2\varepsilon_y\mu_y[(1+\beta^2)\Delta\varepsilon + \varepsilon_y]}{\varepsilon_y}}, \tag{A1}$$

$$k_z^- = \sqrt{\frac{-k_x^2(\Delta\mu + \mu_y) + k_0^2\varepsilon_y\mu_y[(1+\beta^2)\Delta\mu + \mu_y]}{\mu_y}}, \tag{A2}$$

where $+$ and $-$ denote two different transmission modes. Each of two wave vector components $k_z^\pm$ is associated with an eigenwave determined by the null space of the Hamiltonian formalism in Eq. (6), given as $\mathbf{E}^\pm = E_0(e_x^\pm, e_y^\pm, e_z^\pm)$, where E_0 is the electric field magnitude for both plus and minus modes, and

$$\begin{bmatrix} e_x^+ \\ e_y^+ \\ e_z^+ \end{bmatrix} = \begin{bmatrix} k_x^2 - k_0^2\varepsilon_y\mu_y \\ -\beta k_0^2\varepsilon_y\mu_y \\ k_x k_z^+ \end{bmatrix}, \begin{bmatrix} e_x^- \\ e_y^- \\ e_z^- \end{bmatrix} = \begin{bmatrix} -\beta k_z^- \\ k_z^- \\ \beta k_x \end{bmatrix}. \tag{A3}$$

The corresponding magnetic fields are also obtained from the constitutive relation and Maxwell's equations as $\mathbf{H}^\pm = \omega^{-1}\bar{\mu}^{-1}\mathbf{k}\times\mathbf{E}^\pm = \frac{E_0}{\eta_0}(h_x^\pm, h_y^\pm, h_z^\pm)$, where $\eta_0 = \sqrt{\mu_0/\varepsilon_0}$, and

$$\begin{bmatrix} h_x^+ \\ h_y^+ \\ h_z^+ \end{bmatrix} = k_0\varepsilon_y \begin{bmatrix} \beta k_z^+ \\ -k_z^+ \\ -\beta k_x \end{bmatrix},$$
$$\begin{bmatrix} h_x^- \\ h_y^- \\ h_z^- \end{bmatrix} = \frac{1}{k_0\mu_y} \begin{bmatrix} k_x^2 - k_0^2\varepsilon_y\mu_y \\ -\beta k_0^2\varepsilon_y\mu_y \\ k_x k_z^- \end{bmatrix}. \tag{A4}$$

We consider the first-order paraxial approximation of a Gaussian beam propagating with the incident wave number $k_i = k_0 = k_x/\sin\theta_i$, then two vector components $k_z^\pm$ are simplified as q_e and q_o:

$$q_e = \sqrt{\frac{(-\sin^2\theta_i + \varepsilon_y\mu_y)\varepsilon_x}{\varepsilon_y}}, \tag{A5}$$

$$q_o = \sqrt{\frac{(-\sin^2\theta_i + \varepsilon_y\mu_y)\mu_x}{\mu_y}}. \tag{A6}$$

Utilizing the boundary conditions [62] and considering the paraxial approximation, the Fresnel reflection coefficients determined by the incident and reflected amplitudes: $r_{pp} = E_r^p/E_i^p$, $r_{ss} = E_r^s/E_i^s$, $r_{ps} = E_r^p/E_i^s$, and $r_{sp} = E_r^s/E_i^p$, are obtained as

$$r_{pp} = \frac{-q_e + \varepsilon_x\cos\theta_i}{q_e + \varepsilon_x\cos\theta_i}, \tag{A7}$$

$$r_{ss} = \frac{-q_o + \mu_x\cos\theta_i}{q_o + \mu_x\cos\theta_i}, \tag{A8}$$

$$r_{ps} = \frac{2\frac{k_{iy}}{k_i}\sqrt{\varepsilon_x\mu_x}(\sqrt{\varepsilon_x\mu_x} - \sqrt{\varepsilon_y\mu_y})\cot\theta_i}{(q_e + \varepsilon_x\cos\theta_i)(q_o + \mu_x\cos\theta_i)}, \tag{A9}$$

$$r_{sp} = \frac{2\frac{k_{iy}}{k_i}\sqrt{\varepsilon_x\mu_x}\left(\sqrt{\varepsilon_y\mu_y} - \sqrt{\varepsilon_x\mu_x}\right)\cot\theta_i}{(q_e + \varepsilon_x\cos\theta_i)(q_o + \mu_x\cos\theta_i)}, \tag{A10}$$

where r_{pp}, r_{ss}, and $r_{ps}(r_{sp})$ represent the Fresnel reflection coefficients for parallel, perpendicular, and crossing polarization, respectively.

APPENDIX B: THE EXPRESSIONS OF GH AND IF SHIFTS

Here, we will detailedly derive the expressions of GH and IF shifts when a Gaussian beam impinges on the planar interface of Dirac metamaterial. To obtain the GH shift more precisely, the reflection coefficients are expanded as a polynomial of k_{ix} and remained to the first order:

$$r_A(k_{ix}) = r_A(k_{ix} = 0) + k_{ix}\left[\frac{\partial r_A(k_{ix})}{\partial k_{ix}}\right]_{k_{ix}=0}, \tag{B1}$$

where $A \in \{pp, ss\}$. Then the reflection matrix can be written as

$$\begin{bmatrix} r_{pp} - k_{rx}\frac{\partial r_{pp}}{\partial k_{rx}} & r_{ps} \\ r_{sp} & r_{ss} - k_{rx}\frac{\partial r_{ss}}{\partial k_{rx}} \end{bmatrix}, \tag{B2}$$

where ∂k_{rx} can be replaced by $k_0\partial\theta$. In the above equation, the boundary condition $k_{rx} = k_{ix}$ has been introduced.

After replacing the reflection matrix in Eq. (15) with Eq. (B2), the reflected angular spectrum can be written as

$$\begin{aligned}\tilde{E}_r = \exp\left[-\frac{w_0{}^2\left(k_{rx}{}^2 + k_{ry}{}^2\right)}{4}\right] \\ \times\left\{\hat{\mathbf{x}}_r\left[f_p r_{pp}\left(1 - \frac{k_{rx}}{k_0}\frac{\partial\ln r_{pp}}{\partial\theta_i}\right) + f_s\frac{k_{ry}}{k_0}r'_{ps}\right]\right. \\ \left.+\hat{\mathbf{y}}_r\left[f_s r_{ss}\left(1 - \frac{k_{rx}}{k_0}\frac{\partial\ln r_{ss}}{\partial\theta_i}\right) + f_p\frac{k_{ry}}{k_0}r'_{sp}\right]\right\},\end{aligned} \tag{B3}$$

where $r'_{ps} = r_{ps}k_0/k_{ry}$, $r'_{sp} = r_{sp}k_0/k_{ry}$, the boundary condition $k_{ry} = k_{iy}$ has also been introduced. By utilizing the Fourier transformation in Eq. (17), the general expression of the reflected field for GH shift in positon space can be written as

$$\begin{aligned}\mathbf{E}_r \propto \exp\left(ik_0 z_r - \frac{k_0}{2}\frac{x_r^2 + y_r^2}{z_R + iz_r}\right) \\ \times\left\{\hat{\mathbf{x}}_r\left[f_p r_{pp}\left(1 - \frac{ix_r}{z_R + iz_r}\frac{\partial\ln r_{pp}}{\partial\theta_i}\right) + f_s r'_{ps}\frac{iy_r}{z_R + iz_r}\right]\right. \\ \left.+\hat{\mathbf{y}}_r\left[f_s r_{ss}\left(1 - \frac{ix_r}{z_R + iz_r}\frac{\partial\ln r_{ss}}{\partial\theta_i}\right) + f_p r'_{sp}\frac{iy_r}{z_R + iz_r}\right]\right\},\end{aligned} \tag{B4}$$

where $z_R = k_0 w_0^2/2$ is the Rayleigh length. After substituting Eq. (B4) into Eq. (18) and making a further derivation, the GH shifts for horizontal polarization can be obtained as

$$D_{\mathrm{GH}} = \frac{2z_R R_{pp}^2 \varphi_{pp}}{R_{sp}'^2 + 2k_0 z_R R_{pp}^2 + \chi_{pp}} - z_r \frac{2R_{pp}^2 \rho_{pp}}{R_{sp}'^2 + 2k_0 z_R R_{pp}^2 + \chi_{pp}}, \tag{B5}$$

where $r_A = R_A \exp(i\phi_A)$, $\rho_A = \mathrm{Re}(\partial \ln r_A/\partial\theta_i)$, $\varphi_A = \mathrm{Im}(\partial \ln r_A/\partial\theta_i)$, and $\chi_A = R_A^2(\varphi_A^2 + \rho_A^2)$. The GH shift of vertical polarization can be obtained in the same way. The result shows that, in above equation, we can replace the r_{pp} and r_{sp} with r_{ss} and r_{ps}, respectively. In Eq. (B5), the first term denotes the spatial GH shift and the second term represents the angular GH shift which is z_r dependent. Therefore the GH shift can be divided into spatial and angular shifts:

$$\Delta_{\mathrm{GH}}^H = \frac{2z_R R_{pp}^2 \varphi_{pp}}{R_{sp}'^2 + 2k_0 z_R R_{pp}^2 + \chi_{pp}}, \tag{B6}$$

$$\Theta_{\mathrm{GH}}^H = -\frac{2R_{pp}^2 \rho_{pp}}{R_{sp}'^2 + 2k_0 z_R R_{pp}^2 + \chi_{pp}}. \tag{B7}$$

Then for IF shift, we consider that the rotation of polarization for each angular spectrum component is different after reflecting from the interface of Dirac metamaterial. Therefore the reflected polarization states related to the incident polarization state can be written as [64]

$$\begin{bmatrix} r_{pp} - \frac{k_{ry}(r_{ps}-r_{sp})\cot\theta_i}{k_0} & r_{ps} + \frac{k_{ry}(r_{pp}+r_{ss})\cot\theta_i}{k_0} \\ r_{sp} - \frac{k_{ry}(r_{pp}+r_{ss})\cot\theta_i}{k_0} & r_{ss} - \frac{k_{ry}(r_{ps}-r_{sp})\cot\theta_i}{k_0} \end{bmatrix}. \tag{B8}$$

Eliminating the second-order small amount $k_{ry}(r_{ps} - r_{sp})\cot\theta_i/k_0$, the reflection matrix can be rewritten as

$$\begin{bmatrix} r_{pp} & r_{ps} + \frac{k_{ry}(r_{pp}+r_{ss})\cot\theta_i}{k_0} \\ r_{sp} - \frac{k_{ry}(r_{pp}+r_{ss})\cot\theta_i}{k_0} & r_{ss} \end{bmatrix}. \tag{B9}$$

Through the combination of Eqs. (B9), (15), and (16), the general expression of the reflected field for IF shift is determined and can be obtained as

$$\begin{aligned} \tilde{E}_r = \exp\left[-\frac{w_0{}^2\left(k_{rx}{}^2 + k_{ry}{}^2\right)}{4}\right] \\ \times \left\{\hat{\mathbf{x}}_r\left[f_p r_{pp} + f_s \frac{k_{ry}}{k_0} r_{ps}' + f_s \frac{k_{ry}(r_{pp}+r_{ss})}{k_0}\cot\theta_i\right]\right. \\ \left. + \hat{\mathbf{y}}_r\left[f_s r_{ss} + f_p \frac{k_{ry}}{k_0} r_{sp}' - f_p \frac{k_{ry}(r_{pp}+r_{ss})}{k_0}\cot\theta_i\right]\right\}, \end{aligned} \tag{B10}$$

After performing the Fourier transformation, the reflected field in position space can be given as

$$\begin{aligned} \mathbf{E}_r \propto \exp\left(ikz_r - \frac{k_0}{2}\frac{x_r^2 + y_r^2}{z_R + iz_r}\right) \\ \times \left\{\hat{\mathbf{x}}_r\left[f_p r_{pp} + f_s \frac{iy_r}{z_R + iz_r} r_{ps}' + f_s \frac{iy_r(r_{pp}+r_{ss})}{z_R + iz_r}\cot\theta_i\right]\right. \\ \left. + \hat{\mathbf{y}}_r\left[f_s r_{ss} + f_p \frac{iy_r}{z_R + iz_r} r_{sp}' - f_p \frac{iy_r(r_{pp}+r_{ss})}{z_R + iz_r}\cot\theta_i\right]\right\}. \end{aligned} \tag{B11}$$

We consider an incident beam with left-handed circular polarization. The spatial and angular shifts can be obtained by substituting Eq. (B11) into Eq. (19):

$$\Delta_{\mathrm{IF}}^L = \frac{2z_R[\xi_1 - \xi_2 + \zeta\cot\theta_i]}{R_{ps}'^2 + R_{sp}'^2 + 2k_0 z_R\left(R_{pp}^2 + R_{ss}^2\right)}, \tag{B12}$$

$$\Theta_{\mathrm{IF}}^L = \frac{\varsigma_1 - \varsigma_2}{R_{ps}'^2 + R_{sp}'^2 + 2k_0 z_R\left(R_{pp}^2 + R_{ss}^2\right)}, \tag{B13}$$

where $\xi_1 = R_{sp}' R_{ss}\cos(\phi_{sp} - \phi_{ss})$, $\xi_2 = R_{ps}' R_{pp}\cos(\phi_{ps} - \phi_{pp})$, $\varsigma_1 = R_{sp}' R_{ss}\sin(\phi_{sp} - \phi_{ss})$, $\varsigma_2 = R_{ps}' R_{pp}\sin(\phi_{ps} - \phi_{pp})$, $\zeta = R_{pp}^2 + R_{ss}^2 + 2R_{pp}R_{ss}\cos(\phi_{pp} - \phi_{ss})$, and $r_A = R_A\exp(i\phi_A)$. We note that $\phi_{sp} - \phi_{ss} \approx \pi$, $\phi_{ps} - \phi_{pp} \approx 0$, hence $\varsigma_1 \approx 0$, $\varsigma_2 \approx 0$. According to the Eq. (B13), the IF angular shift for left-handed circular polarization is almost zero, that is $\Theta_{\mathrm{IF}}^L \approx 0$. Similarly, we can also get the IF shift for the incident beam with right-handed circular polarization as $\Delta_{\mathrm{IF}}^R = -\Delta_{\mathrm{IF}}^L$ and $\Theta_{\mathrm{IF}}^R = -\Theta_{\mathrm{IF}}^L \approx 0$. Hence, for both left-handed circular polarization and right-handed circular polarization, there is nearly no IF angular shift occurs at the interface of the Dirac metamaterial.

[1] F. Goos and H. Hänchen, Ann. Phys. **436**, 333 (1947).
[2] K. Artmann, Ann. Phys. **437**, 87 (1948).
[3] F. I. Fedorov, J. Opt. **15**, 014002 (2013).
[4] C. Imbert, Phys. Rev. D **5**, 787 (1972).
[5] J. W. Ra, H. L. Bertoni, and L. B. Felsen, SIAM J. Appl. Math. **24**, 396 (1973).
[6] H. M. Lai, S. W. Chan, and W. H. Wong, J. Opt. Soc. Am. A **23**, 3208 (2006).
[7] A. Aiello and J. P. Woerdman, arXiv:0903.3730.
[8] M. Merano, A. Aiello, M. P. Van Exter, and J. P. Woerdman, Nat. Photonics **3**, 337 (2009).
[9] M. Merano, N. Hermosa, A. Aiello, and J. P. Woerdman, Opt. Lett. **35**, 3563 (2010).
[10] Z. Xiao, H. Luo, and S. Wen, Phys. Rev. A **85**, 053822 (2012).
[11] A. Aiello and J. P. Woerdman, Opt. Lett. **33**, 1437 (2008).
[12] A. Aiello, M. Merano, and J. P. Woerdman, Phys. Rev. A **80**, 061801(R) (2009).
[13] M. Merano, N. Hermosa, J. P. Woerdman, and A. Aiello, Phys. Rev. A **82**, 023817 (2010).
[14] K. Y. Bliokh and A. Aiello, J. Opt. **15**, 014001 (2013).
[15] M. P. Aráujo, S. De Leo, and G. G. Maia, Phys. Rev. A **93**, 023801 (2016).
[16] M. P. Aráujo, S. De Leo, and G. G. Maia, Phys. Rev. A **95**, 053836 (2017).
[17] S. Grosche, M. Ornigotti, and A. Szameit, Opt. Express **23**, 30195 (2015).
[18] S. Grosche, A. Szameit, and M. Ornigotti, Phys. Rev. A **94**, 063831 (2016).

[19] M. Merano, Opt. Lett. **41**, 5780 (2016).
[20] W. J. M. Kort-Kamp, N. A. Sinitsyn, and D. A. R. Dalvit, Phys. Rev. B **93**, 081410(R) (2016).
[21] S. Chen, C. Mi, L. Cai, M. Liu, H. Luo, and S. Wen, Appl. Phys. Lett. **110**, 031105 (2017).
[22] W. Wu, S. Chen, C. Mi, W. Zhang, H. Luo, and S. Wen, Phys. Rev. A **96**, 043814 (2017).
[23] X. Yin, L. Hesselink, Z. Liu, N. Fang, and X. Zhang, Appl. Phys. Lett. **85**, 372 (2004).
[24] X. Yin and L. Hesselink, Appl. Phys. Lett. **89**, 261108 (2006).
[25] L. Salasnich, Phys. Rev. A **86**, 055801 (2012).
[26] D. Felbacq, A. Moreau, and R. Smaâli, Opt. Lett. **28**, 1633 (2003).
[27] D. Felbacq and R. Smaâli, Phys. Rev. Lett. **92**, 193902 (2004).
[28] T. Paul, C. Rockstuhl, C. Menzel, and F. Lederer, Phys. Rev. A **77**, 053802 (2008).
[29] I. V. Soboleva, V. V. Moskalenko, and A. A. Fedyanin, Phys. Rev. Lett. **108**, 123901 (2012).
[30] Q. Kong, H.-Y. Shi, J.-L. Shi, and X. Chen, Opt. Express **27**, 11902 (2019).
[31] H. Wu, Q. Luo, H. Chen, Y. Han, X. Yu, and S. Liu, Phys. Rev. A **99**, 033820 (2019).
[32] H. Lai and S. Chan, Opt. Lett. **27**, 680 (2002).
[33] L.-G. Wang, H. Chen, and S.-Y. Zhu, Opt. Lett. **30**, 2936 (2005).
[34] R.-G. Wan and M. S. Zubairy, Phys. Rev. A **101**, 023837 (2020).
[35] C. W. J. Beenakker, R. A. Sepkhanov, A. R. Akhmerov, and J. Tworzydło, Phys. Rev. Lett. **102**, 146804 (2009).
[36] S.-Y. Lee, J. Le Deunff, M. Choi, and R. Ketzmerick, Phys. Rev. A **89**, 022120 (2014).
[37] Q.-D. Jiang, H. Jiang, H. Liu, Q.-F. Sun, and X. C. Xie, Phys. Rev. Lett. **115**, 156602 (2015).
[38] L. Wang and S.-K. Jian, Phys. Rev. B **96**, 115448 (2017).
[39] Y. Wang, H. Li, Z. Cao, T. Yu, Q. Shen, and Y. He, Appl. Phys. Lett. **92**, 061117 (2008).
[40] T. Yu, H. Li, Z. Cao, Y. Wang, Q. Shen, and Y. He, Opt. Lett. **33**, 1001 (2008).
[41] T. Shui, W. X. Yang, Q. Y. Zhang, X. Liu, and L. Li, Phys. Rev. A **99**, 013806 (2019).
[42] T. Sakata, H. Togo, and F. Shimokawa, Appl. Phys. Lett. **76**, 2841 (2000).
[43] A. Kar, N. Goswami, and A. Saha, Appl. Opt. **56**, 9656 (2017).
[44] D. Xu, S. He, J. Zhou, S. Chen, S. Wen, and H. Luo, Appl. Phys. Lett. **116**, 211103 (2020).
[45] W. Wu, W. Zhang, S. Chen, X. Ling, W. Shu, H. Luo, S. Wen, and X. Yin, Opt. Express **26**, 23705 (2018).
[46] W. J. Chen, S. J. Jiang, X. D. Chen, B. Zhu, L. Zhou, J. W. Dong, and C. T. Chan, Nat. Commun. **5**, 5782 (2014).
[47] C. He, C. X. C. Sun, X. P. Liu, M. H. Lu, Y. Chen, L. Feng, and Y. F. Chen, Proc. Natl. Acad. Sci. USA **113**, 4924 (2016).
[48] A. Slobozhanyuk, S. H. Mousavi, X. Ni, D. Smirnova, Y. S. Kivshar, and A. B. Khanikaev, Nat. Photon. **11**, 130 (2017).
[49] S.-Y. Xu, I. Belopolski, N. Alidoust, M. Neupane, G. Bian, C. Zhang, R. Sankar, G. Chang, Z. Yuan, C.-C. Lee, S.-M. Huang, H. Zheng, J. Ma, D. S. Sanchez, B. Wang, A. Bansil, F. Chou, P. P. Shibayev, H. Lin, S. Jia, and M. Z. Hasan, Science **349**, 613 (2015).
[50] B. Yang, Q. Guo, B. Tremain, L. E. Barr, W. Gao, H. Liu, and S. Zhang, Nat. Commun. **8**, 97 (2017).
[51] M. Xiao, Q. Lin, and S. Fan, Phys. Rev. Lett. **117**, 057401 (2016).
[52] Z. K. Liu, B. Zhou, Y. Zhang, Z. J. Wang, H. M. Weng, D. Prabhakaran, and Z. Hussain, Science **343**, 864 (2014).
[53] H. X. Wang, L. Xu, H. Y. Chen, and J. H. Jiang, Phys. Rev. B **93**, 235155 (2016).
[54] Q. Guo, B. Yang, L. Xia, W. Gao, H. Liu, J. Chen, Y. Xiang, and S. Zhang, Phys. Rev. Lett. **119**, 213901 (2017).
[55] F. Liu, J. Xu, G. Song, and Y. Yang, J. Opt. Soc. Am. B **30**, 1167 (2013).
[56] G. Ye, W. Zhang, W. Wu, S. Chen, W. Shu, H. Luo, and S. Wen, Phys. Rev. A **99**, 023807 (2019).
[57] L. Lu, C. Fang, L. Fu, S. G. Johnson, J. D. Joannopoulos, and M. Soljacic, Nat. Phys. **12**, 337 (2016).
[58] H.-X. Wang, Y. Chen, Z. H. Hang, H.-Y. Kee, and J.-H. Jiang, npj Quantum Mater. **2**, 54 (2017).
[59] W. Xu, Q. Yang, G. Ye, W. Wu, W. Zhang, H. Luo, and S. Wen, Phys. Rev. A **101**, 023826 (2020).
[60] Q. Guo, O. You, B. Yang, J. B. Sellman, E. Blythe, H. Liu, Y. Xiang, J. Li, D. Fan, J. Chen, C. T. Chan, and S. Zhang, Phys. Rev. Lett. **122**, 203903 (2019).
[61] J. Lekner, J. Phys.: Condens. Matter **3**, 6121 (1991).
[62] P. H. Chang, C. Y. Kuo, and R. L. Chern, Opt. Express **22**, 25710 (2014).
[63] M. Born and F. Wolf, *Principles of Optics: Electromagnetic Theory of Propagation, Interference and Diffraction of Light* (Elsevier, New York, 2013).
[64] H. Luo, X. Zhou, W. Shu, S. Wen, and D. Fan, Phys. Rev. A **84**, 043806 (2011).
[65] X. Zhou, Z. Xiao, H. Luo, and S. Wen, Phys. Rev. A **85**, 043809 (2012).
[66] X. Zhou, X. Ling, H. Luo, and S. Wen, Appl. Phys. Lett. **101**, 251602 (2012).
[67] F. Krayzel, R. Pollès, A. Moreau, M. Mihailovic, and G. Granet, J. Eur. Opt. Soc. Rapid Publ. **5**, 10025 (2010)
[68] R. Pollès, M. Mihailovic, E. Centeno, and A. Moreau, Phys. Rev. A **94**, 063808 (2016).